Comparison of rotating finite range model and Thomas-Fermi fission barriers in the $A\sim190$ mass region

K. Mahata,* S. Kailas, and U. K. Pal†
Nuclear Physics Division, Bhabha Atomic Research Centre, Mumbai 400 085, India
(Received 30 August 2003; published 31 December 2003)

Statistical model calculations have been performed using the rotating finite range and the Thomas-Fermi models for fission barriers. The results have been compared with the existing cross sections for ^{40}Ar+^{148}Sm and ^{86}Kr+^{104}Ru systems. Analyses show that the use of Thomas-Fermi fission barrier without any shell correction gives the best fit to the experimental cross sections. This observation is in contrast to the conclusion drawn from γ-ray fold measurements for ^{48}Ca+^{142}Nd and ^{80}Se+^{110}Pd systems reported earlier.

DOI: 10.1103/PhysRevC.68.067603 PACS number(s): 25.70.Jj, 24.75.+i, 24.10.Pa

The fission barrier (B_f) plays a crucial role in heavy-ion induced fusion-fission dynamics. Variety of phenomena, e.g., fast fission, quasifission, preequilibrium fission, superdeformation, K isomer, have been observed depending on the height and position of the fission barrier. The formation of the compound nucleus depends on whether the initial composite system of the target and the projectile is more compact than the fission saddle shape. After the equilibrated compound nucleus is formed, the competition between the fission and the particle evaporation channel is strongly influenced by the height of the fission barrier. In addition, the fission fragment angular distribution $\mathcal{W}(\theta)$ is sensitive to the effective moment of inertia at the saddle point ($\mathfrak{I}_{eff}$) which is related to the saddle point shape. The effective moment of inertia is defined as $1/\mathfrak{I}_{eff}=1/\mathfrak{I}_{\parallel}-1/\mathfrak{I}_{\perp}$, where $\mathfrak{I}_{\parallel}$ and $\mathfrak{I}_{\perp}$ are the moment of inertia for rotation at the saddle point along and perpendicular to the symmetry axis, respectively. The availability of new experimental data has always brought refinement to the theoretical estimation of the fission barrier. Initially the rotating liquid drop model (RLDM) [1] provided a simple understanding of the fission phenomena. Fission barrier heights from this prescription had to be reduced by a factor varying between 0.5 and 0.9 to explain the fission-evaporation residue cross sections. The values of $\mathfrak{I}_{eff}$ deduced from the fission fragment angular distributions of actinide targets were found to be larger than the RLDM predictions [2]. This discrepancy was partially removed by the use of the rotating finite range model (RFRM) [3]. The RFRM fission barriers with a scaling factor around unity (0.90–1.10) give good explanation of the available fission-evaporation cross sections. This model has also removed the discrepancy between the deduced $\mathfrak{I}_{eff}$ values and the predictions for actinide targets [4]. However, recent studies using preactinide targets [5,6] showed disagreement between the RFRM predictions and the deduced values of $\mathfrak{I}_{eff}$.

Recently, Djerroud *et al.* [7] have reported a measurement of γ-ray fold distributions for ^{48}Ca+^{142}Nd and ^{80}Se+^{110}Pd systems leading to same compound nucleus (^{190}Hg) and at same excitation energy ($E^*\approx37$ MeV). The statistical model calculations were performed using the Gilbert-Cameron [8] level density prescription with a level density parameter $a_n=A/8.0$ MeV^{-1} and the RFRM fission barriers. According to the predictions of the statistical model calculations an enhanced population of high spin states was expected for the most mass symmetric system, due to large coupled channel effect. This expected enhancement was not consistent with the experimental observation. Surprisingly, the experimental γ-ray fold distributions for the $2n$ evaporation residue (ER) for both the systems were similar. The above discrepancy between the model prediction and the experiment was interpreted as arising due to inaccuracy of the fission barrier used in the calculations. The experimental fold distributions were explained by statistical model calculations using the Thomas-Fermi fission barrier [9] with a shell correction (ε_S) of −3 MeV. However, the authors did not demonstrate the corresponding sensitivity of the ER and the fission cross sections to the statistical model parameters. It will be interesting to investigate this aspect, viz., sensitivity of ER and fission cross sections to the RFRM and the Thomas-Fermi fission barrier.

The experimental fission and ER cross sections are not available for the above mentioned systems. The fission and the ER excitation functions are available for ^{40}Ar+^{148}Sm system [10], which has a mass asymmetry similar to that of ^{48}Ca+^{142}Nd system and forms a compound nucleus (^{188}Hg), two neutrons away from ^{190}Hg [7]. The evaporation residue cross sections are also available for ^{86}Kr+^{104}Ru system [11], which populates ^{190}Hg with a mass asymmetry similar to that of ^{80}Se+^{110}Pd system. In the present work, detailed statistical model calculations have been performed for ^{40}Ar+^{148}Sm and ^{86}Kr+^{104}Ru systems to investigate the sensitivity of the ER and the fission cross sections to the statistical model parameters, in particular the fission barrier.

Statistical model analyses were performed using the statistical model code PACE [12] using the experimental masses and shell corrected level densities. An energy dependent shell correction [13] of the level density parameter, $a_n=\tilde{a}[1+(\delta W/U)(1-e^{-\eta U})]$, with an asymptotic value $\tilde{a}=A/8$ MeV^{-1} and a damping factor $\eta=0.054$ MeV^{-1} was employed. The ground state shell correction δW is the difference between

*Electronic address: kmahata@magnum.barc.ernet.in
†Present address: Max-Planck-Institut für Kernphysik, Saupfercheckweg 1, 69117 Heidelberg, Germany.

TABLE I. The parameter sets used in statistical model analyses.

Parameter set	B_f	ε_S (MeV)
A	RFRM	0.0
B	0.85×RFRM	0.0
C	Thomas-Fermi	0.0
D	Thomas-Fermi	−3.0

the liquid drop and the experimental mass defects. U is defined as $U=E^*-E_{rot}(J)-\Delta_p$, where $E_{rot}(J)$ and Δ_p are the rotational energy and the pairing energy, respectively. The yrast line obtained from the RFRM was suitably modified to match the experimentally known yrast line of ^{188}Hg. The level density parameter at the saddle deformation (a_f) was obtained as $a_n(a_f/a_n)$, where a_f/a_n is the ratio of level density parameter at the saddle deformation to that at the equilibrium deformation. As discussed in Ref. [5] the same ground state shell correction (δW) was applied for the level density parameter at the saddle point. Statistical model predictions using four different fission barriers, given in Table I, were compared with the above mentioned data. The ratio of level density parameter, a_f/a_n, was taken to be unity.

The Thomas-Fermi fission barriers are not readily available in a parametrized form for use in statistical model calculation. In view of this we have used the same parametric form as in Ref. [7],

$$B_f(J) = B_f(0)e^{-J^2/2\sigma_J^2} + \varepsilon_S,$$

where $B_f(0)=14$ MeV and $\sigma_J=27\hbar$. The parameter ε_S represents the difference in the shell correction at the saddle point and the equilibrium configuration. The above mentioned fission barrier parameters were obtained by fitting the microscopically calculated Thomas-Fermi fission barrier for ^{190}Hg [7]. In the present study the same parameters for the Thomas-Fermi fission barriers have been assumed for both the compound nuclei (^{188}Hg and ^{190}Hg) and successive decay products. The Thomas-Fermi fission barriers at zero spin [14] for ^{188}Hg and ^{190}Hg are comparable. We have also used $\varepsilon_S=-3.0$ MeV for both the compound nuclei and the successive decay products. Angular momentum dependence of different fission barriers used for ^{190}Hg are compared in Fig. 1. As can be seen from Fig. 1, a drastic lowering of the fission barrier results due to inclusion of a shell correction of −3.0 MeV.

In the case of the ^{40}Ar+^{148}Sm system, the spin distributions of the compound nucleus, required for the statistical model calculations, were obtained from CCDEF [15] calculations which fits the fusion excitation function. The same channels as those of Ref. [10] were coupled to reproduce the fusion excitation function. As shown in Fig. 2, the statistical model predictions with $B_f=0.85\times$RFRM (parameter set *B*) agree reasonably well with the data for the ^{40}Ar+^{148}Sm system. Use of the Thomas-Fermi fission barrier (parameter set *C*) also gives a good agreement between the data and the statistical model predictions. Inclusion of a shell correction of −3.0 MeV in the Thomas-Fermi fission barriers (parameter set *D*), as suggested in Ref. [7] from γ-ray fold distribution measurements, produces a large discrepancy between the data and the statistical model predictions (see Fig. 2).

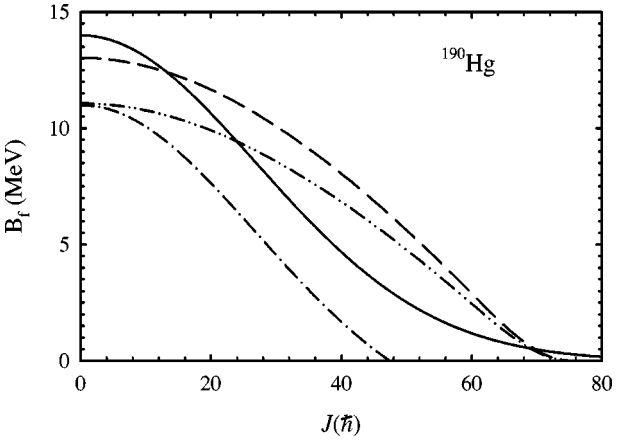

FIG. 1. Fission barriers as a function of angular momentum for ^{190}Hg as calculated by the RFRM (dashed line) and the Thomas-Fermi model (continuous line). The dash-dotted line is the Thomas-Fermi fission barrier with a shell correction of −3 MeV. The dot-dot-dashed line is the RFRM fission barrier scaled by a factor of 0.85.

Although only the evaporation residue excitation function is available for ^{86}Kr+^{104}Ru system, it contains information on the fissionability of the nuclei involved as demonstrated in Ref. [11]. A dimensionless quantity $(\sigma_{ER}/\pi\lambda\!\!\!^{-2})^{1/2}$ versus $E_{\text{c.m.}}$ has been plotted, where σ_{ER} is the ER cross section and $\lambda\!\!\!^{-}$ is the reduced de Broglie wavelength in the entrance channel. The useful feature of excitation functions for the quantity $(\sigma_{ER}/\pi\lambda\!\!\!^{-2})^{1/2}$ is that they saturate at sufficiently high excitation energy to a value ℓ_{sat}. The values of ℓ_{sat} vary characteristically with the compound nucleus and are inde-

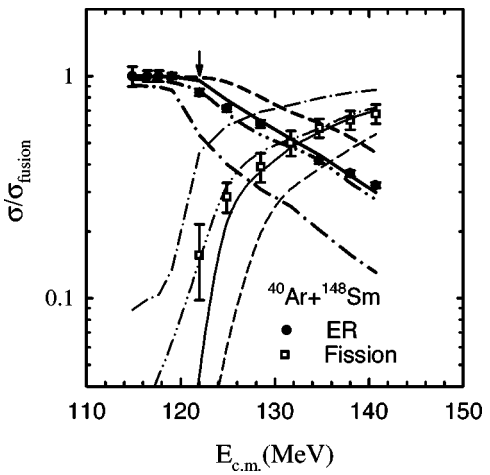

FIG. 2. Fission and ER formation probability (σ/σ_{fusion}) as a function of $E_{\text{c.m.}}$ for ^{40}Ar+^{148}Sm system. The filled circle and the open square represent the ER and the fission cross sections, respectively, from Ref. [10]. The dashed, the dot-dot-dashed, the continuous, and the dash-dotted lines are the fission (thin line) and the ER (thick line) excitation functions using parameter sets *A*, *B*, *C*, and *D* in Table I, respectively. The arrow indicates $E^*=37.8$ MeV, where the entry spin distributions and the other observables in Table II have been calculated (see text).

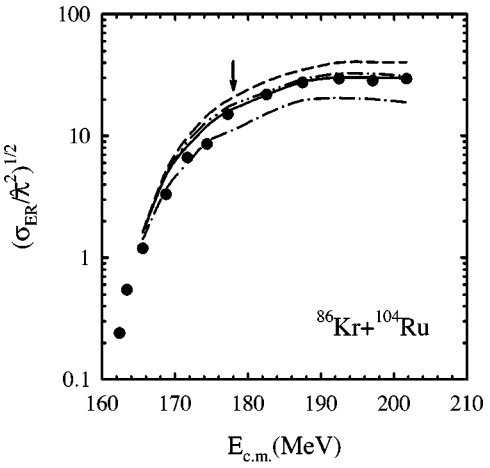

FIG. 3. Comparison of the measured excitation function of $(\sigma_{ER}/\pi\lambda^2)^{1/2}$ (see text) for ^{86}Kr+^{104}Ru system with statistical model calculations using different fission barriers. The dashed, the dot-dot-dashed, the continuous, and the dash-dotted lines correspond to parameter sets *A*, *B*, *C*, and *D* in Table I, respectively. The arrow indicates the same as Fig. 2.

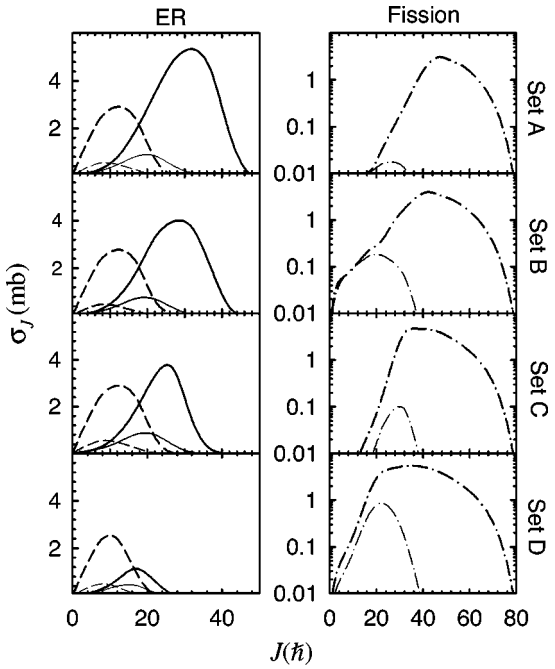

FIG. 4. Variation of the entry spin distributions for 2*n* (continuous lines), 3*n* (dashed lines) evaporation residue and the spin distribution of the fissioning nuclei (dash-dotted lines) with different fission barriers used for ^{40}Ar+^{148}Sm (thin lines) and ^{86}Kr+^{104}Ru (thick lines) systems at E^*=37.8 MeV. The sets *A*, *B*, *C*, and *D* correspond to those in Table I.

pendent of the entrance channel. This implies that the ER cross sections are limited by competition with fission and not by any other fusion hindrance effects [11]. The value of ℓ_{sat} does not depend upon the compound nucleus spin distribution provided the distribution extends to sufficiently large *J* as compared to ℓ_{sat}. The quantity $(\sigma_{ER}/\pi\lambda^2)^{1/2}$ has been calculated using PACE for different fission barriers. As can be seen from Fig. 3, the calculations with set *B* though close to the data are consistently higher. While set *C* provides a good agreement with the data for $E_{c.m.}>175$ MeV, the set *D* yields results which are in good agreement with the data for $E_{c.m.}<175$ MeV. As argued earlier, if the data available only at higher energies are considered (as they are less sensitive to input spin distribution and entrance channel), then set *C* is the best in reproducing the data. Even in this system inclusion of a shell correction of −3.0 MeV, as suggested in Ref. [7] from γ-ray fold distribution measurements, fails to reproduce the data.

In addition, we have calculated several quantities of interest [σ_{ER}, P_f, σ_{3n}/σ_{2n}, $\mathcal{W}(180^\circ)/\mathcal{W}(90^\circ)$] using PACE for both the systems under consideration at E^*=37.8 MeV, where the measurement of fold distributions in Ref. [7] was made. Statistical model calculations using the Thomas-Fermi fission barriers with a shell correction of −3.0 MeV (set *D*), as sug-

TABLE II. Statistical model predictions of evaporation residue cross sections (σ_{ER}), fission barrier height (B_f), fission probability (P_f), ratio of 2*n* to 3*n* evaporation residue cross section (σ_{3n}/σ_{2n}), and fission fragment angular anisotropy [$\mathcal{W}(180°)/\mathcal{W}(90°)$] at E^*=37.8 MeV using different parameter sets. The sets *A*, *B*, *C*, *D* correspond to those in Table I.

Quantity	*A*	*B*	*C*	*D*	Observed
			^{40}Ar+^{148}Sm		
σ_{ER} (mb)	5.0	4.4	4.8	2.8	4.31±0.15 [10]
B_f (J=29) (MeV)	10.3	8.8	7.9	4.9	
P_f (%)	1.43	14.8	4.53	45.6	15.6±6.0 [10]
σ_{3n}/σ_{2n}	0.51	0.51	0.54	0.93	
$\mathcal{W}(180^\circ)/\mathcal{W}(90^\circ)$	3.99	3.51	4.88	3.71	
			^{86}Kr+^{104}Ru		
σ_{ER} (mb)	33.9	26.4	21.9	9.9	19.5±0.57[a] [11]
B_f (J=29) (MeV)	10.3	8.8	7.9	4.9	8.7±0.25 [11]
P_f (%)	28.0	44.0	53.6	79.1	
σ_{3n}/σ_{2n}	0.40	0.53	0.79	2.29	
$\mathcal{W}(180^\circ)/\mathcal{W}(90^\circ)$	8.38	7.27	6.68	5.46	

[a]Interpolated.

gested in Ref. [7], do not agree with the observed quantities in Table II. It has been shown that all these quantities are very sensitive to the fission barrier (Table II). Hence, these quantities can be used to constrain statistical model parameters. The variation of the entry spin distributions for $2n$,$3n$ evaporation residues and the spin distribution of the fissioning nuclei with different fission barriers used for ^{40}Ar+^{148}Sm and ^{86}Kr+^{104}Ru systems at E^*=37.8 MeV is shown in Fig. 4. The predicted entry spin distributions of $2n$ and $3n$ channels for both the systems become similar (see Fig. 4) when the Thomas-Fermi fission barriers with a shell correction of −3.0 MeV are used. However, Thomas-Fermi fission barriers with a shell correction of −3.0 MeV fail to explain the corresponding cross sections as mentioned earlier. As shown in Fig. 4, the spin distributions of the fissioning nuclei are also very sensitive to the fission barriers. The same can be seen in fission fragment angular anisotropy (see Table II), which is a sensitive function of the spin distribution of the fissioning nuclei. In contrast with the results of Ref. [7], we have found significantly large $3n$ ER cross section irrespective of fission barrier used and entrance channel asymmetry (see Table II). In Ref. [7] it was reported that $2n$ channel represents over 90% of the total fusion-evaporation cross section at $E^* \sim 37.8$ MeV.

In summary, we have performed statistical model analyses for ^{40}Ar+^{148}Sm and ^{86}Kr+^{104}Ru systems using the RFRM and the Thomas-Fermi fission barriers. It has been found that the RFRM fission barriers have to be reduced by a factor of 0.85 to get a good agreement between the calculations and the experimental fission-ER cross sections. Use of the Thomas-Fermi fission barriers gives a good agreement between the existing fission-ER cross sections and the calculations. Inclusion of a shell correction of −3.0 MeV in the Thomas-Fermi fission barriers, as suggested in Ref. [7] from γ-ray fold distribution measurements, produces a large discrepancy between the measured cross sections and the statistical model predictions. The γ-ray fold distribution measurements reported in Ref. [7] are not consistent with the fission and the ER cross sections available for the same (^{190}Hg) [11] or a nearby (^{188}Hg) [10] compound nucleus. In contrast with the results reported in Ref. [7] we have shown that the $3n$ channel is significantly large irrespective of the fission barrier used and the entrance channel asymmetry for the systems under consideration at E^*=37.8 MeV. The ER and the fission cross sections are crucial to constrain the statistical model parameters and any conclusions reached regarding presence or absence of shell effects in fission barrier based on γ-ray fold distributions alone will not be reliable.

K.M. wishes to thank A. Navin for fruitful discussions.

[1] S. Cohen, F. Plasil, and W. J. Swiatecki, Ann. Phys. (N.Y.) **82**, 557 (1974).
[2] R. F. Reising, G. L. Bate, and J. R. Huizenga, Phys. Rev. **141**, 1161 (1966).
[3] A. J. Sierk, Phys. Rev. C **33**, 2039 (1986).
[4] R. Vandenbosch, in *Proceedings of the Beijing International Symposium*, on Physics at Tandem, edited by Jiang Chenglie, Li Shounan, Sun Zuzun, and Zang Huanquiao (World Scientific, Singapore, 1986), p. 355.
[5] K. Mahata, S. Kailas, A. Shrivastava, A. Chatterjee, A. Navin, P. Singh, S. Santra, and B. S. Tomar, Nucl. Phys. **A720**, 209 (2003).
[6] K. Mahata, S. Kailas, A. Shrivastava, A. Chatterjee, P. Singh, S. Santra, and B. S. Tomar, Phys. Rev. C **65**, 034613 (2002).
[7] B. Djerroud *et al.*, Phys. Rev. C **61**, 024607 (2000).
[8] A. Gilbert and A. G. W. Cameron, Can. J. Phys. **43**, 1446 (1965).
[9] W. D. Myers and W. J. Swiatecki, Nucl. Phys. **A612**, 249 (1997).
[10] W. Reisdorf *et al.*, Nucl. Phys. **A438**, 212 (1985).
[11] W. Reisdorf *et al.*, Nucl. Phys. **A444**, 154 (1985).
[12] A. Gavron, Phys. Rev. C **21**, 230 (1980).
[13] A. V. Ignatyuk, G. N. Smirenkin, and A. S. Tishin, Sov. J. Nucl. Phys. **21**, 255 (1975).
[14] W. D. Myers and W. J. Swiatecki, Phys. Rev. C **60**, 014606 (1999).
[15] C. H. Dasso and S. Landowne, Comput. Phys. Commun. **26**, 187 (1987); J. Férnandez-Niello, C. H. Dasso, and S. Landowne, *ibid.* **54**, 409 (1989).